Fuel Processing Technology, Volume 223, December 2021, Article number 106998
DOI:10.1016/j.fuproc.2021.106998

Investigation of the hydrodynamics in the regenerator of fluid catalytic cracking unit integrated by chemical looping combustion

Fatih Güleç[1,2]*, Ahmet Erdogan[3], Peter T. Clough[2], Edward Lester[1]

[1]*Advanced Materials Research Group, Faculty of Engineering, University of Nottingham, Nottingham, NG7 2RD, UK.*
[2]*Energy and Power Theme, School of Water, Energy and Environment, Cranfield University, Cranfield, MK43 0AL, UK*
[3]*Mechanical Engineering, Faculty of Engineering, Inonu University, 44280 Malatya, Turkey*
**Corresponding Author: Fatih.Gulec1@nottingham.ac.uk, Gulec.Fatih@outlook.com*

Abstract

Oil refineries are responsible for 4-6 % of global CO_2 emissions, and 20-35 % of these emissions released from the regenerator of Fluid Catalytic Cracking (FCC) units, which are the essential units for the conversion of heavier petroleum residues (vacuum gas oil) into more valuable products. Chemical looping combustion (CLC) has been recently proposed to mitigate the CO_2 emissions released from the regenerator of FCC units with a lower energy penalty. However, a detailed experimental and modelling investigation is still necessary in order to identify the hydrodynamics in the regenerator of chemical looping combustion integrated with fluidised catalytic cracking (CLC-FCC). A computational fluid dynamic (CFD) study was conducted to understand the hydrodynamic behaviours of gas-solid two-phase flow in the regenerator of the CLC-FCC unit, based on a three-dimensional multiphase model (Eulerian-Eulerian) with the kinetic theory of granular flow.

The results provide a useful insight into regenerator hydrodynamics, in terms of oxygen carrier modified FCC catalysts and FCC coke distribution profiles, in the regenerator of CLC-FCC. The conventional drag models (Syamlal-O'Brien and Gidaspow) predict a bed density profiles of a dense phase (250-300 kg/m^3) at the dense phase (0-0.25 of h/H), and a dilution phase from h/H=0.25 to 0.50 of regenerator. The bed density profile is indistinguishable from the industrial data provided for conventional FCC regenerators. The fluidisation gas (CO_2) passes through the centre of the regenerator where the fluidisation gas splits the catalyst particles from the centre to the walls, to create a dilute particle phase in the centre and a dense particle-phase near the wall, which is one of the characteristic flow regimes in circulating fluidised bed reactors. The particles in the centre demonstrate an upward flow trend with a particle velocity above 3.0 m/s while the dense particles near the wall tend to go down with relatively low particle velocity of < 0.5 m/s, which creates vortexes and a non-uniform particle distribution in the regenerator. The distribution of the fluidising gas provides better mixing of solid particles in the entrance and the optimisation of the superficial gas velocities (1.0 m/s) to create a distributed flow regime with developed vortexes through the dense and dilute phases. Furthermore, the laminar and turbulent flow models demonstrated no significant differences in terms of axial bed density profile in the regenerator of the CLC-FCC concept. These findings demonstrated that the hydrodynamics of catalysts in the CLC-FCC regenerator successfully predicted with CFD modelling and the prediction results aligned well with the conventional FCC regenerator.

Keywords: CO_2 Capture, CLC-FCC, Chemical Looping Combustion, Fluid Catalytic Cracking, CFD.

1 Introduction

Fluid Catalytic Cracking (FCC) an essential process for the conversion of heavier petroleum residues [1, 2] such as vacuum gas oil into more valuable light cycle oil (LCO; C_{13}-C_{20}), gasoline (C_5-C_{12}), and LPG (C_3-C_4), but the production of light gases (H_2, C_1-C_2) should be minimised [3, 4]. A commercial FCC unit consists of a catalytic riser reactor and a regenerator [5, 6]. In the riser reactor, the preheated feedstock is injected, vaporised, and mixed with a hot catalyst and steam, with cracking temperatures of 480-600 °C which decrease up to the riser as the endothermic cracking reactions proceed. After the riser reactor, the gas-phase cracked products and catalysts powders are separated in the disengagement zone i.e. a cyclone. The gas-phase products are then sent to a fractional column while the coke deposited catalysts are stripped with steam to remove volatiles and then sent to the regenerator where the coke is combusted with air in a controlled manner at temperatures typically close to 750 °C. After regeneration, coke free catalysts are sent back to the riser; thereby completing the cycle. Combustion of the coke generates heat to sustain the endothermic cracking reactions in the riser, so the system is thermally balanced. The concentration of CO_2 in the flue gas is 12-16 vol. % with a low concentration of CO (~12 ppm), 50-200 vppm of NOx and 300-600 vppm of SOx in the full combustion mode [3, 7].

The regenerator part of the FCC unit is one of the largest CO_2 emitters, about 20-35 %, from a standard refinery [8-10], which is responsible for about 4-6 % of the global CO_2 emissions [11, 12]. Based on the characteristics of the FCC process, it is possible to capture the CO_2 released from the FCC regenerator when combined with post-combustion methods such as amine scrubbing [13, 14]. Such 1st generation post-combustion capture techniques are considered to be relatively mature but there are other processes, notably oxy-combustion [15-17] and chemical looping combustion (CLC) [18-22], that can now offer considerably lower energy penalties. In our previous studies [18, 19, 21], the applicability of CLC for FCC has been experimentally demonstrated with a schematic diagram of the proposed novel CLC-FCC process as in Figure 1a (in Section 2.2). The modification of reduced oxygen carriers with an equilibrium catalyst (ECat) had no significant impact on the cracking of n-hexadecane. Additionally, greater than 90 wt.% combustion of an FCC coke was achieved with CuO, Co_3O_4 and Mn_2O_3 modified ECat at 750 °C for 40–60 min, which is similar to conditions employed in the conventional regenerator of FCC units; 650–750 °C for 30–60 min. Therefore, CLC is a promising technology to incorporate into the next generation of FCC units to optimise CO_2 capture. In addition to CO_2 capture, NO_x emissions would be lower with the application of CLC [23-25]. In this novel CLC–FCC concept, the oxygen carrier in the fresh catalyst would be in a reduced state (Me_nO_{m-1}/Cat: *Cu_2O/Cat, CoO/Cat, Mn_3O_4/Cat*) as it enters the FCC riser reactor. The spent or deactivated catalyst with deposited coke (Coke/Me_nO_{m-1}/Cat: *Coke-Cu_2O/Cat, Coke-CoO/Cat, Coke-Mn_3O_4/Cat*) is then transferred to the regenerator. The reduced state oxygen carrier modified catalysts would also be circulated to the air reactor via another fluidised bed, where the reduced state is oxidised (Me_nO_m/Cat: *CuO/Cat, Co_3O_4/Cat, Mn_2O_3/Cat)*. By mixing the coke deposited catalyst with the oxidised oxygen carrier modified catalyst in the regenerator,

the coke would be oxidised to CO_2 + H_2O resulting in the reduction of the oxidised oxygen carrier as shown in Reaction 33 (in Section 2.2). The reduced oxygen carrier modified catalyst can then be circulated to both the FCC riser reactor (for cracking reaction) and air reactor (for re-oxidation, Reaction 34, in Section 2.2). The concentrated CO_2 released from the regenerator is then captured after the flue gas is separated from the moisture. The net CLC reaction for the coke combustion in the regenerator and air reactor is shown in Reaction 35 (in Section 2.2).

Coke combustion with oxygen carriers may occur by three different mechanisms in the regenerator of the CLC-FCC unit, which operates as a bubbling/turbulent dense fluidised bed [4]. Firstly, the soft coke released from the coke deposited catalyst can combust with the oxygen carriers. Secondly, hard coke can combust with the solid phase oxygen carriers via solid-solid interactions between coke and oxygen carriers. Finally, hard coke combustion occurs with gas-phase oxygen released from the oxygen carriers via chemical-looping resulting from their oxygen uncoupling (CLOU) properties [19, 21]. Previous experiments on the combustion of coke with oxygen carriers demonstrated highly promising results for the application of CLC to the FCC unit as a novel CO_2 capture technology [18-21]. However, there is a need for more empirical work and modelling in order to identify the complex hydrodynamics and reaction mechanisms in the regenerator and the riser reactor of the proposed novel CLC–FCC concept to optimise the design and operation conditions. Computational fluid dynamics (CFD) has, therefore, become one of the most useful approaches in the design, performance analysis, and optimisation of multiple reactors [4]. As hydrodynamics [26] , coke combustion [26-29], and heat transfer [28, 29] in an industrial scale turbulent fluidised bed FCC regenerator have all been accurately predicted using CFD modelling.

In this study, the hydrodynamics of two phases; gas (CO_2) and solids (coke deposited oxygen carrier modified FCC catalyst and oxidised oxygen carrier modified FCC catalysts), in the regenerator of CLC-FCC concept has been investigated based on the Eulerian model with the kinetic theory of granular flow. The effects of fluidisation gas (CO_2) inlet geometry, superficial gas velocity (0.6, 0.7, 0.8, 0.9, 1.0 m/s) and the flow models (turbulent and laminar) were investigated in order to simulate the hydrodynamics of the novel FCC-CLC regenerator using the Syamlal-O'Brien drag model. Furthermore, the simulation results were compared with the other conventional drag models (Schiller-Nauman and Gidaspow), modified drag model in the literature and the industrial data.

2 CFD Model and Simulation Method

2.1. Conversion of Mass and Momentum

The continuity equation for gas and solid phases (subscript q can be gas (g) or solid (s));

$$\frac{\partial}{\partial t}\left(\alpha_q \rho_q\right) + \nabla.\left(\alpha_q \rho_q \overset{\mathrm{r}}{\upsilon}_q\right) = 0 \qquad (1)$$

$$\alpha_g + \alpha_s = 1 \tag{2}$$

The momentum equations for each phase;

$$\frac{\partial}{\partial t}\left(\alpha_g \rho_g \vec{\upsilon}_g\right) + \nabla.\left(\alpha_g \rho_g \vec{\upsilon}_g \vec{\upsilon}_g\right) = -\alpha_g \nabla p_g + \alpha_g \rho_g \vec{g} - \beta\left(\vec{\upsilon}_g - \vec{\upsilon}_s\right) + \nabla.\alpha_g \bar{\bar{\tau}}_g \tag{3}$$

$$\frac{\partial}{\partial t}\left(\alpha_s \rho_s \vec{\upsilon}_s\right) + \nabla.\left(\alpha_s \rho_s \vec{\upsilon}_s \vec{\upsilon}_s\right) = -\alpha_s \nabla p_g - \nabla p_s + \alpha_s \rho_s \vec{g} - \beta\left(\vec{\upsilon}_s - \vec{\upsilon}_g\right) + \nabla.\alpha_s \bar{\bar{\tau}}_s \tag{4}$$

The transport equations of k-ε turbulence model are;

$$\frac{\partial}{\partial t}\left(\alpha_q \rho_q k_q\right) + \nabla.\left(\alpha_q \rho_q \vec{\upsilon}_q k_q\right) = \nabla.\left(\alpha_q\left(\mu_q + \frac{\mu_{t,q}}{\sigma_k}\right)\nabla k_q\right) + \left(\alpha_q G_{k,q} - \alpha_q \rho_q \varepsilon_q\right) + \alpha_q \rho_q \Pi_{k_q} \tag{5}$$

$$\frac{\partial}{\partial t}\left(\alpha_q \rho_q \varepsilon_q\right) + \nabla.\left(\alpha_q \rho_q \vec{\upsilon}_q \varepsilon_q\right) = \nabla.\left(\alpha_q\left(\mu_q + \frac{\mu_{t,q}}{\sigma_\varepsilon}\right)\nabla \varepsilon_q\right) + \alpha_q \frac{\varepsilon_q}{k_q}\left(C_{1\varepsilon} G_{k,q} - C_{2\varepsilon} \rho_q \varepsilon_q\right) + \alpha_q \rho_q \Pi_{\varepsilon_q} \tag{6}$$

where, G_{kq} is the production of turbulent kinetic energy, the turbulent viscosity of each phase can be calculated;

$$\mu_{t,q} = \rho_q C_\mu k_q^2 / \varepsilon_q \tag{7}$$

The standard $k-\varepsilon$ model constants [30] are;

$$C_{1\varepsilon} = 1.44,\ C_{2\varepsilon} = 1.92,\ \sigma_k = 1.0,\ \sigma_\varepsilon = 1.3 \tag{8}$$

The solid phase fluctuations are described via the kinetic theory of granular flow [31, 32]. The granular temperature (Θ) is defined to be proportional to the kinetic energy of the random motions of solid particles. The solid phase pressure and viscosities can be determined as a function of granular temperature. The transport equation for granular temperature [33] is;

$$\frac{\partial}{\partial t}\left(\alpha_s \rho_s \Theta\right) + \nabla.\left(\alpha_s \rho_s \Theta \vec{\upsilon}_s\right) = \frac{2}{3}\left[\left(-p_s \bar{\bar{I}} + \bar{\bar{\tau}}_s\right) : \nabla.\vec{\upsilon}_s + \nabla.\left(\Gamma_\Theta \nabla \Theta\right) - \gamma_s + \phi_{gs}\right] \tag{9}$$

The two terms on the right-hand side of the equation are the energy generated by the solid stress tensor and the diffusive flux of granular energy. The interphase drag coefficient can be determined by the Syamlal-O'Brien (Equations 10-14), Schiller-Nauman (Equations 15-17), Gidaspow drag models (Equations 18-20) [34-37];

$$\beta = \frac{3\rho_g \alpha_g \alpha_s \left|\vec{\upsilon}_g - \vec{\upsilon}_s\right|}{4\upsilon_{r,s}^2 d_s} C_D\left(\frac{\mathrm{Re}_s}{\upsilon_{r,s}}\right) \tag{10}$$

$$C_D = \left(0.63 + 4.8/\left(\mathrm{Re}_s / \upsilon_{r,s}\right)^{1/2}\right)^2 \tag{11}$$

$$\mathrm{Re}_s = \rho_g \alpha_g \left|\vec{\upsilon}_g - \vec{\upsilon}_s\right| d_s / \mu_g \tag{12}$$

$$\upsilon_{r,s} = 0.5\left(A - 0.06\,\mathrm{Re}_s + \left(\left(0.06\,\mathrm{Re}_s\right)^2 + 0.12\,\mathrm{Re}_s\left(2B - A\right) + A^2\right)^{1/2}\right) \tag{13}$$

$$A = \alpha_g^{4.14},\ B = \begin{pmatrix} 0.8\alpha_g^{1.28} & \alpha_g \le 0.85 \\ \alpha_g^{2.65} & \alpha_g > 0.85 \end{pmatrix} \tag{14}$$

$$\beta = \frac{3}{4} C_D \frac{\alpha_s \rho_g \left| \vec{\upsilon}_s - \vec{\upsilon}_g \right|}{d_s} \tag{15}$$

$$C_D = \begin{cases} \dfrac{24}{\mathrm{Re}_s}(1 + 0.15\,\mathrm{Re}_s^{0.687}) & (\mathrm{Re}_s \le 1000) \\ 0.44 & (\mathrm{Re}_s > 1000) \end{cases} \tag{16}$$

$$\mathrm{Re}_s = \frac{\alpha_g \rho_g d_s \left| \vec{\upsilon}_s - \vec{\upsilon}_g \right|}{\mu_g} \tag{17}$$

$$\beta = \begin{cases} \dfrac{3}{4} C_D \dfrac{\alpha_s \alpha_g \rho_g \left| \vec{\upsilon}_s - \vec{\upsilon}_g \right|}{d_s} \alpha_g^{-2.65} & (\alpha_g > 0.8) \\ 150 \dfrac{\alpha_s (1-\alpha_g) \mu_g}{\alpha_g d_s^2} + 1.75 \dfrac{\alpha_s \rho_g \left| \vec{\upsilon}_s - \vec{\upsilon}_g \right|}{d_s} & (\alpha_g \le 0.8) \end{cases} \tag{18}$$

$$C_D = \frac{24}{\alpha_g \mathrm{Re}_s} \left[1 + 0.15 (\alpha_g \mathrm{Re}_s)^{0.687} \right] \tag{19}$$

$$\mathrm{Re}_s = \frac{\rho_g d_s \left| \vec{\upsilon}_s - \vec{\upsilon}_g \right|}{\mu_g} \tag{20}$$

The gas-phase stress tensor is expressed as

$$\bar{\bar{\tau}}_g = \mu_{t,g} \left[\nabla \vec{\upsilon}_g + \left(\nabla \vec{\upsilon}_g \right)^T \right] + \left(\lambda_g - 2/3 * \mu_{eff,g} \right) \nabla \vec{\upsilon}_g \bar{\bar{I}} \tag{21}$$

The solid-phase pressure is expressed as

$$p_s = \alpha_s \rho_s \Theta \left[1 + 2 g_0 \alpha_s \left(1 + e \right) \right] \tag{22}$$

The radial distribution function that modifies the probability of particles collisions as solid-phase becomes dense and is presented as

$$g_0 = \left[1 - \left(\alpha_s / \alpha_{s,\max} \right)^{1/3} \right]^{-1} \tag{23}$$

The granular temperature is defined as

$$\Theta = 1/3 * \left(\overline{\upsilon' \upsilon'} \right) \tag{24}$$

The solid-phase stress tensor is evaluated from

$$\bar{\bar{\tau}}_s = \lambda_s \nabla . \vec{\upsilon}_s \bar{\bar{I}} + \mu_s \left[\nabla \vec{\upsilon}_s + \left(\nabla . \vec{\upsilon}_s \right)^T \right] - 2/3 * \left(\nabla . \vec{\upsilon}_s \right) \bar{\bar{I}} \tag{25}$$

The solid-phase bulk viscosity (λ_s) [38] is defined as;

$$\lambda_s = 4/3 * \alpha_s^2 \rho_s d_s g_0 \left(1 + e \right) \left(\Theta / \pi \right)^{1/2} \tag{26}$$

The shear viscosity of solid particles (μ_s) is evaluated using the Syamlal model [34-37];

$$\mu_s = \frac{4}{5}\alpha_s \rho_s d_s g_0 (1+e)\left(\frac{\Theta}{\pi}\right)^{1/2} + \frac{\alpha_s \rho_s d_s (\pi\Theta)^{1/2}}{6(3-e)}\left[1+\frac{2}{5}\alpha_s g_0 (1+e)(3e-1)\right] \quad (27)$$

Given the physical properties of FCC catalyst particles and the relatively dilute flow, the drag term is evaluated using the conventional drag models (Syamlal-O'Brien, Schiller-Nauman, Gidaspow). For similar reasons, as well as the fact that the drag model should be suitable as a shear model, the best choice of solid particles shear viscosity model is Syamlal.

The collisions dissipation energy (γ_s) [38] is defined as

$$\gamma_s = 3(1-e^2)\alpha_s^2 \rho_s g_0 \Theta\left(\frac{4}{d_s}\left(\frac{\Theta}{\pi}\right)^{1/2} - \nabla.\vec{\upsilon}_s\right) \quad (28)$$

The coefficient of granular diffusion (Γ_Θ) [39] is given by

$$\Gamma_\Theta = \frac{150\rho_s d_s (\pi\Theta)^{1/2}}{384(1+e)g_0}\left[1+\frac{5}{6}(1+e)g_0\alpha_s\right]^2 + 2\alpha_s^2\rho_s d_s g_0 (1+e)\left(\frac{\Theta}{\pi}\right)^{1/2} \quad (29)$$

The transfer of fluctuating kinetic energy (ϕ_{gs}) [39] is defined as

$$\phi_{gs} = -3\beta\Theta \quad (30)$$

In Eulerian–Eulerian approach of modeling multiphase turbulent flows, the turbulent dispersion force takes into account the interphase turbulent momentum transfer. The turbulent dispersion force is expressed as a turbulent diffusion and is developed by averaging the interphase drag term. Turbulent dispersion is evaluated by the Simonin model [40];

$$\beta\left(\vec{\upsilon}_s - \vec{\upsilon}_g\right) = \beta\left(\vec{U}_s - \vec{U}_g\right) + \beta\left(\frac{D_s}{0.75\alpha_s}\nabla\alpha_s - \frac{D_g}{0.75\alpha_g}\nabla\alpha_g\right) \quad (31)$$

$$D_g = \frac{2}{3}k_s\left(\frac{b+\eta_{gs}}{1+\eta_{gs}}\right)\eta_{gs}\tau_{F,gs} + \left[\frac{2}{3}k_s + \frac{2}{3}bk_s\left(\frac{b+\eta_{gs}}{1+\eta_{gs}}\right)\right]\tau_{F,gs} \quad (32)$$

$$D_s = \frac{2}{3}k_g\left(\frac{b+\eta_{sg}}{1+\eta_{sg}}\right)\eta_{sg}\tau_{F,sg} + \left[\frac{2}{3}k_s + \frac{2}{3}bk_g\left(\frac{b+\eta_{sg}}{1+\eta_{sg}}\right)\right]\tau_{F,sg} \quad (33)$$

$$\eta_{gs} = 0.27\beta k_s \Big/ \alpha_g\varepsilon_s(2\rho_g+\rho_s)\left(1+\frac{3}{2}(1.8-1.35\cos^2\theta)\frac{\left(\vec{\upsilon}_g - \vec{\upsilon}_s\right)^2}{k_s}\right)^{1/2} \quad (34)$$

$$b = 1.5\left(\rho_s/\rho_g + 0.5\right)^{-1} \quad (35)$$

$$\tau_{F,sg} = \frac{\alpha_s\rho_s}{\beta}\left(\frac{\rho_s}{\rho_g}+0.5\right) \quad (36)$$

$$\Pi_k = \frac{\beta}{\alpha_g \rho_g}\left\{2k_g\left(\frac{b+\eta_{sg}}{1+\eta_{sg}}\right) - 2k_g - \left(\overset{\mathrm{r}}{\upsilon}_g - \overset{\mathrm{r}}{\upsilon}_s\right)\left[\frac{D_s}{0.75\alpha_s}\nabla\alpha_s - \frac{D_g}{0.75\alpha_g}\nabla\alpha_g\right]\right\} \quad (37)$$

$$\Pi_\varepsilon = C_{3\varepsilon}\left(\frac{\varepsilon_g}{k_g}\right)\Pi_k \quad (38)$$

The turbulence model constant ($C_{3\varepsilon}$) equals 1.2 in the applied turbulence model.

2.2. Regenerator geometry

Chang et al. [26, 27] and Gao et al. [41] investigated the effects of regenerator conditions on the hydrodynamics and coke regeneration in a turbulent fluidised bed regenerator from a commercial FCC unit in China, having a processing capacity of 70,000 tons per year. In order to make a better justification and comparison, the same turbulent fluidised bed regenerator was modified and scaled down (1:10) in all directions (Figure 1b) for the application of CFD to the regenerator of the CLC-FCC concept (Figure 1a). The applicability of CLC for FCC unit has been recently demonstrated at lab-scale [18, 19, 21]; however, there is neither a pilot nor a commercial application of this concept to validate the results from this study. Therefore, the previous CFD studies on conventional FCC regenerator would guide to make a better justification for the hydrodynamic properties in the regenerator of the CLC-FCC concept. The modified regenerator consists of three stages: a lower (diameter of 2.1 m and length of 7.92 m), a middle (diameter of 2.7 m and length of 3.5 m), and an upper stage (diameter of 2.96 m and length of 5.86 m) [26]. The spent catalysts (Coke/Cu_2O/ECat) and the oxidised oxygen carriers modified catalysts (CuO/ECat) are fed to the regenerator in the middle of the lower stage. By the mixing of Coke/Cu_2O/ECat and CuO/ECat in the regenerator, the coke on catalysts would be oxidised to CO_2 and H_2O while the oxidised oxygen carrier (CuO/ECat) reduced to Cu_2O/ECat. The regenerated catalysts (Cu_2O/ECat) are removed from the bottom of the regenerator. The bed was fluidised with pure CO_2. The particles which left the regenerator from the top are recirculated with the external cyclones back to the spent catalyst feed line.

Although there is a wide range of FCC design, the regenerator of a conventional FCC unit is usually defined as a bubbling fluidised bed that consists of two regions: the dense phase and the dilute phase [42]. At the velocities of 0.6–1.2 m/s in an industrial regenerator, the bulk catalyst particles stay in the dense phase, immediately above the air distributor and the dilute phase could be defined as one or more regions above the dense phase up to the cyclone inlet, and has a substantially lower catalyst concentration [42]. For example, an industrial regenerator provided a dense phase (~285 kg/m^3 at the bottom of regenerator), a dilute phase (~145 and ~60 kg/m^3 in the middle zone) and a highly dilute phase (~12 kg/m^3 at the top of the regenerator) [26].

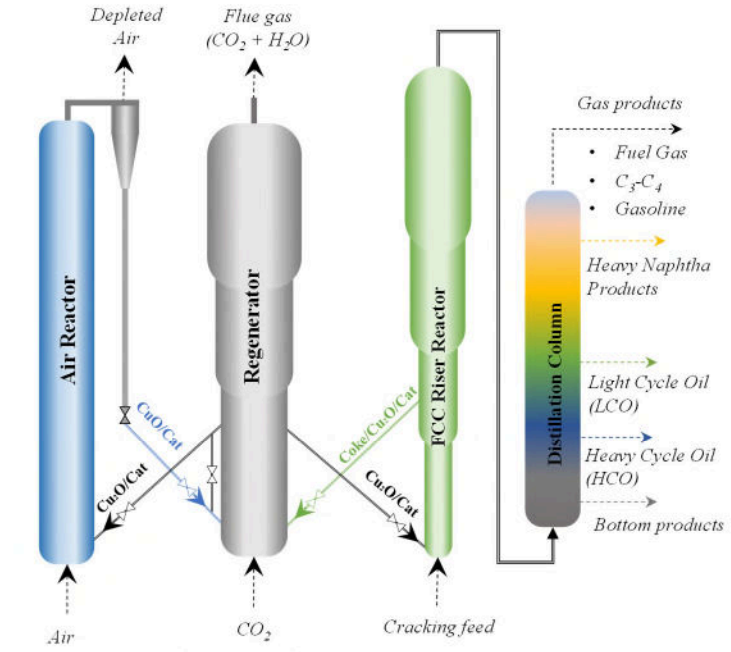

a) Proposed CLC-FCC concept

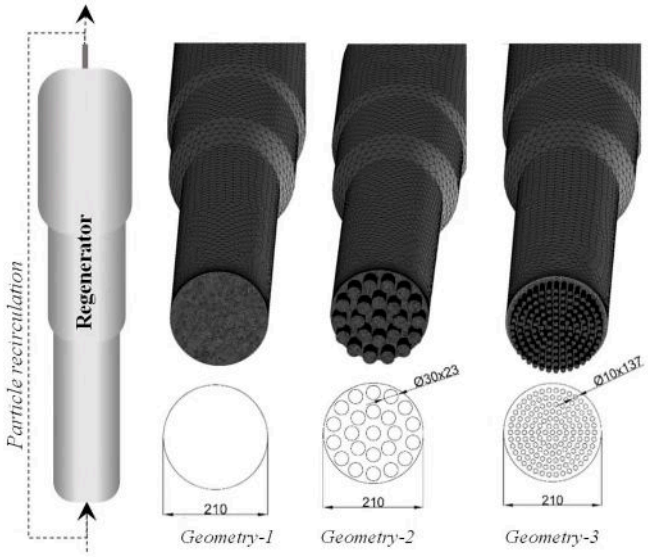

b) Regenerator and inlet geometries for CFD

Figure 1. Schematic diagram of a) proposed novel CLC-FCC process [19-21, 43] and b) regenerator geometry used in the CFD study [26, 27, 41].

The coke combustion reactions in the regenerator;

$$4CuO_{(s)} + Coke_{(s)} \rightarrow 2Cu_2O_{(s)} + CO_{2(g)} \qquad \Delta H_r^0 = -101.5\ kJ/mol \qquad (33)$$

The metal oxidation reactions in the air reactor;

$$2Cu_2O_{(s)} + O_{2(g)} \rightarrow 4CuO_{(s)} \qquad \Delta H_0^0 = -292.0\ kJ/mol \qquad (34)$$

The net reaction in the regenerator and air reactor;

$$Coke_{(s)} + O_{2(g)} \rightarrow CO_{2(g)} \qquad \Delta H_C^0 = -393.5\ kJ/mol \qquad (35)$$

ΔH_r^0 and ΔH_0^0 are the standard heats of reaction for the reduction and oxidation at 298 K and 1 atm.

2.3. Operating conditions

A case study is conducted with an assumption of a commercial size of CLC-FCC unit having a Vacuum Gas Oil (VGO) feed rate of 50000 barrels per day (bpd) to simulate the hydrodynamics in the regenerator. The catalyst flowrates (Coke/Cu_2O/ECat, CuO/ECat, and Cu_2O/ECat) were then determined using the mass balance on the potential CLC-FCC unit. The conversion of VGO to LPG, Gasoline, and LCO was assumed to be 85.6 wt.% [5]. The cracking reaction of VGO over the Cu_2O/ECat and associated product distributions were taken from Sadeghbeigi [5] but updated using the experimental results presented in our previous studies [19, 21]. These are presented in the Appendix (Table A1). The catalyst flowrates were then updated according to the scale reduction in the regenerator for the CFD analysis (shown in Table 1) with the operating conditions.

Table 1. Operating conditions of the regenerator of the CLC-FCC concept.

Variables	Unit	Value	References
Regenerator pressure	kPa	250	[27]
CO_2 inlet temperature	°C	200	[44]
Coke deposited catalyst inlet temperature	°C	527	[45]
Oxygen carrier modified catalyst inlet temperature	°C	750	[44]
Regenerated catalyst outlet temperature	°C	750	[44]
Regenerator inventory (re-scaled)	kg	8.50	[27]
Oxygen carrier modified catalyst flowrate	g/s	28.69 (CuO/ECat)	-
Spent catalyst mass flowrate	g/s	11.30 (Coke/Cu_2O/ECat*)	-
Coke in spent catalyst flowrate	g/s	0.59 (Coke)	[21]
Carbon content in spent catalyst	wt%	0.98	[21]
Ratio of H/C in the coke	wt/wt	0.075	[21]
Regenerated catalyst	-	Cu_2O/ECat	[21]
Oxygen carrier for combustion	-	CuO/ECat$^+$ (12 % of CuO)	[21]
Stochiometric ratio of CuO/Coke$^\#$	-	1.0	[19, 21]

*Cracking catalyst (ECat) is modified 11.2 % of Cu_2O [21].
$^+$ Coke deposited on Cu_2O/ECat can be combusted with the stoichiometrically required amount of CuO (12%) modified with ECat [19-21].
$^\#$The stoichiometric ratio of CuO to coke was assumed as 1.0, which supports the stoichiometrically required oxygen released from the CuO to combust the coke.

2.4. Boundary and initial conditions

The solid geometries of the analysed numerical models were created in the SolidWorks package program with a scale-down of 1:10 in all directions. The reason for the scale down was to reduce the calculation time, data storage and to create a model that could be validated by future experiments at lab-scale. Numerical flow analyses were performed by transferring the model geometries to the ANSYS package program. As shown in Figure 1, the "velocity inlet", "pressure outlet", and "wall" boundary conditions are defined for the lower inlet section of the regenerator (excluding inlet geometry analysis), upper outlet section, and all other surfaces, respectively. The CFD simulation parameters are also presented in Table 2.

Table 2. CFD simulation parameters of the regenerator.

Variable	Unit	Value/Condition	References
Gas-solid model	-	Eulerian-Eulerian with kinetic theory	[27, 41, 45]
Wall boundary condition	-	No-slip for gas, partial-slip for solids	[27, 41]
Restitution coefficients	-	0.95	[27, 45]
Specularity coefficient	-	0.6	[27]
Timestep	s	5.0×10^{-4}	[26]
Max number of iterations per time step	-	20	[4, 26]
Superficial gas velocity	m/s	0.6, 0.7, 0.8, 0.9, 1.0	[42]
Convergence criteria	-	1×10^{-3}	[4, 26, 45]
Pressure velocity coupling	-	Simple	[4, 26, 45]
Max solid packing volume fraction	-	0.63	[21, 41, 45]
Discretisation Scheme	-	First-order upwind	[45]
Particle density[+]	kg/m^3	1560	[46]
Particle diameter of catalysts[+]	μm	65	[21, 26]

[+] Particle density and particle diameter were assumed the same for all the solid particles in the regenerator (Coke/Cu_2O/ECat, CuO/ECat, Cu_2O/ECat) [21].

A tetrahedral mesh was created for Geometry-3 for the grid sensitivity analysis in which four different grids (M1-155×10^3 cells, M2-215×10^3 cells, M3-300×10^3 cells, and M4-415×10^3 cells) were investigated. The mesh was refined in all of flow domain. The medium option is chosen for mesh smoothing and the span angle of the mesh curvature is 18 degrees. The relevance canter and mesh smoothing are coarse and medium, respectively. In order to obtain more sensitivity solutions in the inlet region of the flow domain, dense mesh is created near the CO_2 inlet surface. Maximum face and edge sizing of the mesh at the inlet surface is 2 mm for all geometries and simulation. In the flow domains, the maximum element size is 35 mm for M1, 27 mm for M2, 21 mm for M3 and 17 mm for M4. The growth rate is 1.2. Skewness value which plays an important role determining mesh quality. The maximum skewness value of a negligible number of the mesh is ~0.8, which is stated as acceptable value while the average skewness value of a large number of mesh is ~0.2 stated essential value. Furthermore, to investigate the effects of fluidisation gas distribution geometry, three different geometries were designed, where the fluidisation gas (CO_2) flows into the regenerator through a single pipe with a 210 mm diameter (Geometry-1), 23 pipes each with a diameter of 30 mm (Geometry-2) and 137 pipes each with a diameter of 10 mm (Geometry-3) (presented in Figure 1b). Through the fluidisation gas inlet geometry analysis, the "mass flow inlet" boundary condition is defined at the inlet surface to keep an equal amount of CO_2 feed to the regenerator with all geometries. Furthermore, the effect of superficial gas velocity on the hydrodynamics in the regenerator was investigated using five different superficial gas velocities (0.6, 0.7, 0.8, 0.9, 1.0 m/s) with Geometry-3 under a turbulent flow regime The minimum fluidisation velocity and Reynold numbers under superficial gas velocities are provided in the appendix. Different drag models such as Schiller-Nauman [47], Gidaspow [48], and Syamlal-O'Brien [37] were also simulated with Geometry-3 under a turbulent flow regime at a superficial gas velocity of 1.0 m/s. To identify the flow regime, Geometry-3 was simulated under both turbulent and laminar flow regimes at a superficial gas velocity of 1.0 m/s. The simulation results were

validated using industrial data (bed density profiles) and the improved drag model results published by Chang et al. [26] which uses a geometry correction factor and a bed height ratio (h/H) instead of bed height. The simulations were conducted using catalysts in the regenerator inventory with a given catalyst mass fraction and bed height assuming the mass of catalyst withdrawn from the regenerator is equal to the mass of catalyst inject to the regenerator. The transient state flow was applied to all the analysis. The simulations were performed up to 10 s in real-time as the system was found to generally reach hydrodynamic equilibrium after 5-6 s.

Although the density changes on the commercial FCC catalyst due to the modification of oxygen carriers was taken into consideration in the CFD model, the agglomeration, attrition, and sintering problems were neglected regarding the relevant information in the literature. As in our previous publication [21, 43], the CuO modified ECat catalysts demonstrated relatively low agglomeration and sintering under the operating conditions of FCC regenerator < 800 °C for a maximum 45 min of residence time. Furthermore, using supported Cu, both sintering and agglomeration problems of CuO can be solved [49-51]. For example, neither sintering nor agglomeration was demonstrated for CuO supported on Al_2O_3 prepared by co-precipitation [18, 52].

3 Results and Discussions

3.1. Grid independency

To determine appropriate mesh numbers, a grid sensitivity analysis was investigated using four different mesh numbers (M1-155×10^3 cells, M2-215×10^3 cells, M3-300×10^3 cells, and M4-415×10^3 cells) at a superficial gas velocity of 1.0 m/s. Figure 2 demonstrates the comparison of these four different grids as a function of time-averaged particle volume fraction through radial distribution at a height of 250 mm and 500 mm for a simulation time of 10 s. Additionally, the particle volume fraction profiles for four different grids for 4 s and 8 s are presented in Figure 3.

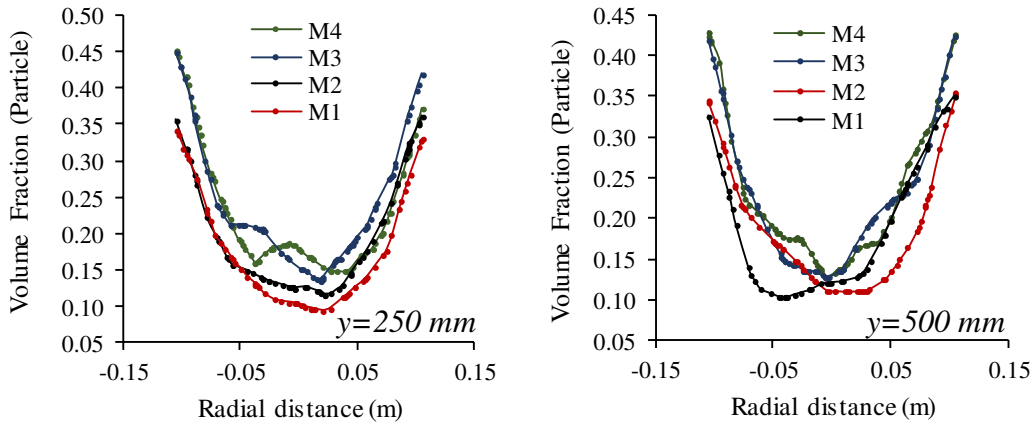

Figure 2. Time-averaged particle volume fraction through radial distribution at the height of 250 mm and 500 mm for four different grids at the superficial gas velocity of 1.0 m/s.

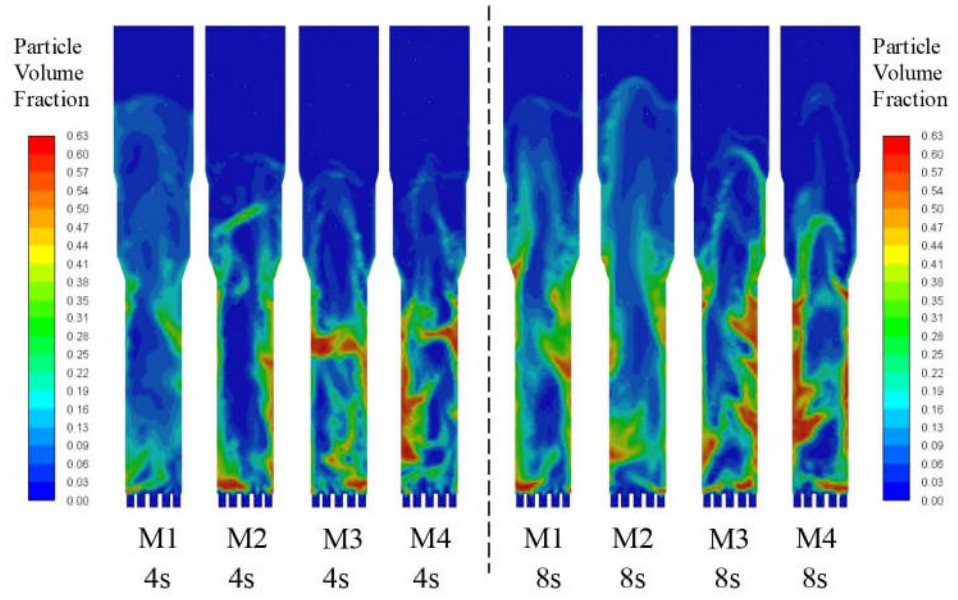

Figure 3. Particle volume fraction profiles for four different grids at 4 s and 8 s at the superficial gas velocity of 1.0 m/s.

The radial distribution of solid volume fraction for the fine mesh (M4) and medium mesh (M3) demonstrate very similar trends at 250 and 500 mm of height in the bed (Figure 2). Furthermore, the particle volume fraction profiles (Figure 3) also visually show the similarity between Mesh 3 and Mesh 4 at 4-8 s of simulation with irregular shapes. The medium mesh (M3-300×10^3 cells) is sufficiently fine to provide reasonably grid-independent results for the hydrodynamics in the regenerator. Furthermore, it demonstrates a lower computational run time compared to finer meshes such as Mesh-4. The Mesh-3 (300×10^3 cells) was therefore selected as the base case mesh number and applied in the rest of the simulation work.

3.2. Comparison of drag models and validation

The drag force plays crucial roles in the hydrodynamics of gas-solid phases [53]. To predict flow patterns and interactions of gas-solid phases, various drag models were developed for the fluidised beds such as Schiller-Nauman [47], Gidaspow [48], Syamlal-O'Brien [37] and these drag models were modified by Gao et al. [41, 54] and Chang et al. [26, 27] for the application of the FCC regenerator. Figure 4 shows the axial bed density profiles for the CLC-FCC regenerator simulated by different drag models of Schiller-Nauman [47], Gidaspow [48], and Syamlal-O'Brien [37]. The results were also compared with the improved drag model results provided by Chang et al. [26] and the industrial data using bed density profiles with unitless bed height ratio (h/H).

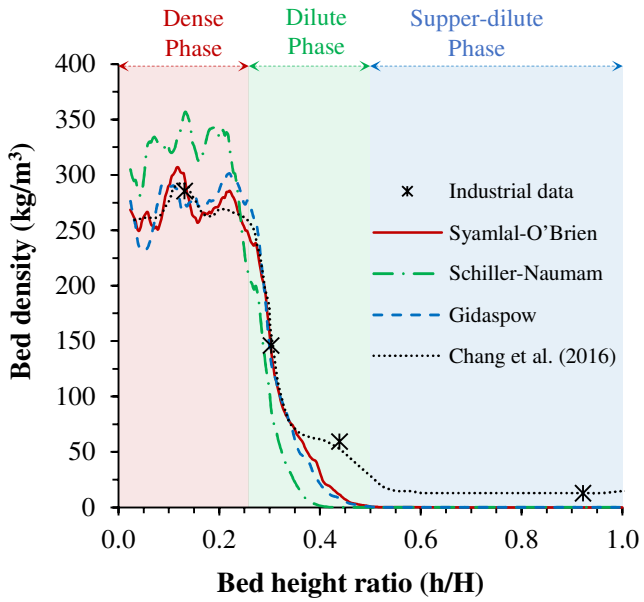

Figure 4. Axial bed density profiles for the CLC-FCC regenerator produced by different drag models, and comparison with improved drag models and industrial data [26]. The drag models of Syamlal-O'Brien, Schiller-Nauman, Gidaspow were applied to the CLC-FCC regenerator.

The industrial data of bed density could be divided into three sections: a dense phase (~285 kg/m^3 at h/H of 0.13), a dilute phase (~145 and ~60 kg/m^3 at h/H of 0.30 and 0.43) and a highly dilute phase (~12 kg/m^3 at h/H of 0.92) [26]. Although the conventional drag models (Syamlal-O'Brien, Schiller-Nauman, Gidaspow) fail to predict the hydrodynamics of the catalyst particles in the regenerator of the conventional FCC unit [26, 41], Figure 4 shows that the conventional drag models provide similar trends with the industrial data: a dense phase at the bottom of the regenerator (h/H of 0-0.25), a dilute phase in the middle of the regenerator (h/H of 0.25-0.50). In the dense phase and the first part of the dilute phase (h/H<0.35), the Syamlal-O'Brien and Gidaspow drag models estimated similar axial bed densities (250-300 kg/m^3) with the industrial data and improved drag model provided by Chang et al. [26]. Conversely the Schiller-Naumam drag models overestimated the bed densities (300-350 kg/m^3) in the dense phase resulting in a slight underestimation in the dilute phase. Both models provide a better prediction of hydrodynamics in the higher density circulating fluidized bed riser [55] and fluidised bed reactor with FCC catalysts [56].

However, these three conventional drag models all underestimated the bed densities in the second part of the dilute phase (0.35<h/H) and through the highly dilute phase compared to the conventional FCC regenerator. This underestimation could be attributed to the increase in the density of commercial FCC catalyst after the modification of oxygen carrier. As the density of CuO (6.31 g/cm^3) is relatively higher than the density of commercial FCC catalyst (ECat, 2.70 g/cm^3). The modification of commercial FCC catalyst with CuO increase the density of new CLC-FCC catalyst [43]. The increase in the density results a resistance to fluidisation and more catalysts located in the dense phase instead of dilute phases.

Therefore, it is not clear that the reason of the underestimation in dilute phase is whether because of the physicochemical changes on the new CLC-FCC catalyst or the drag models.

Gidaspow and Syamlal-O'Brien drag models could therefore be applicable and validated drag models for the prediction of hydrodynamics in the dense phase of the CLC-FCC regenerator while they can be modified for a better prediction in the highly dilute phase. Among conventional drag models, Syamlal-O'Brien drag model was therefore used in order to identify the hydrodynamics of gas-solid interaction in the regenerator of CLC-FCC unit for the following simulations.

3.3. Distribution of fluidisation gas

Figure 5 demonstrates the time-averaged particle volume fraction through radial distribution at the height of 250, 500, and 750 mm for the different fluidisation gas inlet geometries. Figure 6 also shows the instantaneous particle volume fraction profiles for these geometries (single entrance and multi entrances) for Mesh-3 for 1-10 s. The geometries (G1, G2 and G3) demonstrates similar and nearly axisymmetric radial distribution based on the time-averaged volume fraction, as seen in Figure 5. The particle volume fractions demonstrate a decrease through the column from bottom to top, which proves the dense phase at the bottom and dilute phases at the top of the regenerator. The particles mostly concentrate near the wall (0.05 – 0.1 m), while the volume fraction was the lowest around the central zone (-0.05 m – 0.05 m).

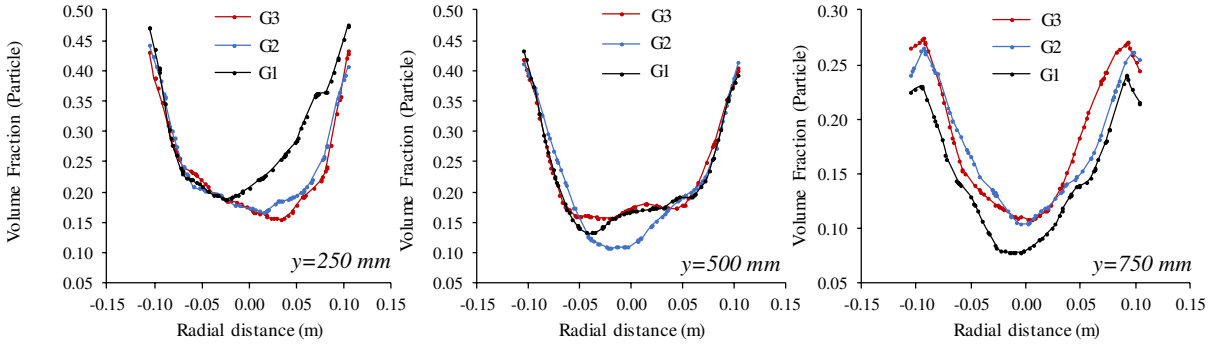

Figure 5. Time-averaged particle volume fraction through radial distribution for different inlet geometries at the regenerator height of 250, 500, and 750 mm.

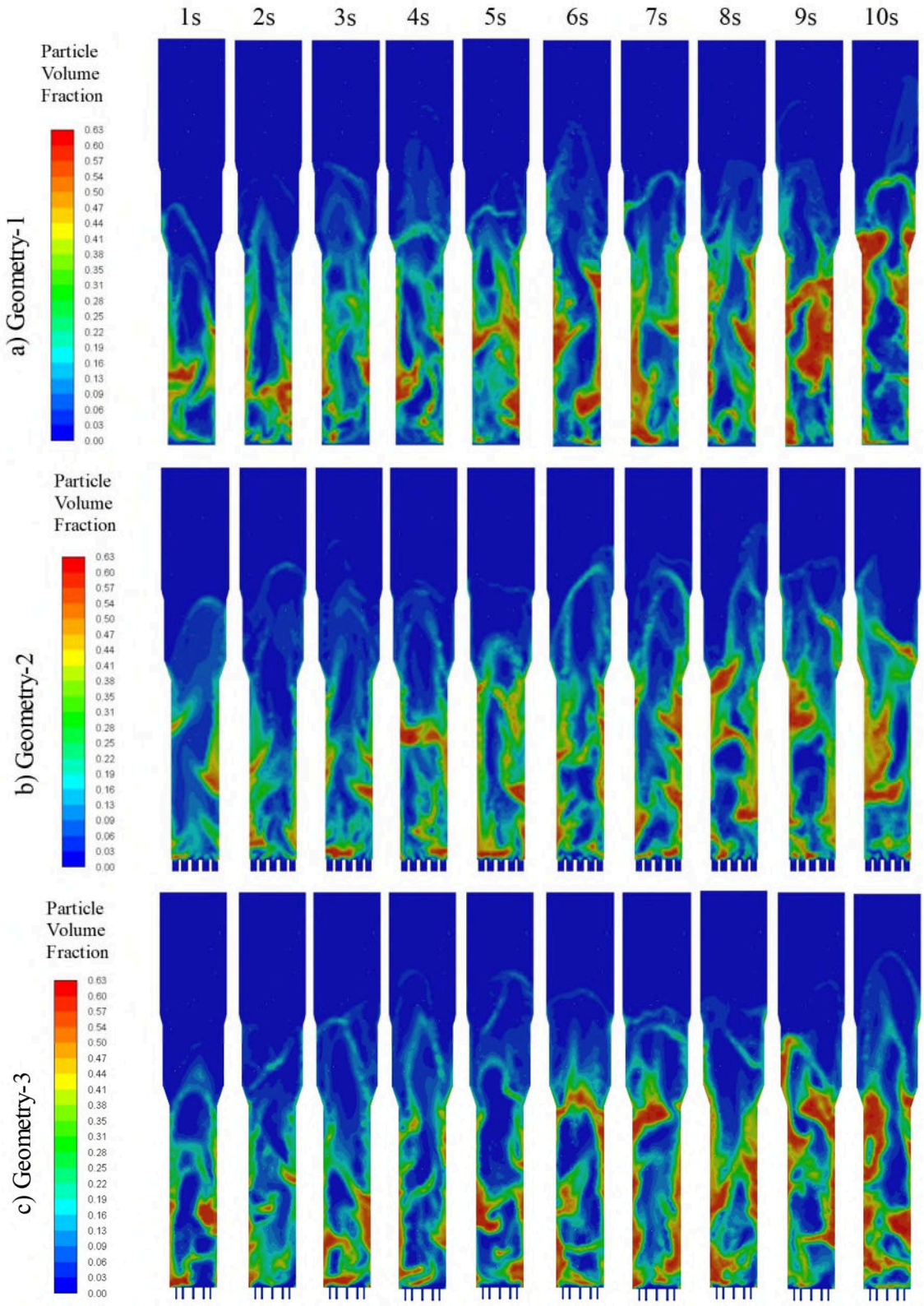

Figure 6. Instantaneous particle volume fraction profiles for different inlet geometries at Mesh-3 for 10 s.

The instantaneous particle volume fractions after 6-7 s demonstrate similar profiles for each geometry (Figure 6), which could be attributed to a steady-state condition in the regenerator. Most of the particles are generally located near the wall (as also presented in Figure 5), whilst fewer particles are found in

the centre of the regenerator, which may be attributed to the flow of fluidisation gas (CO_2) from the centre of the geometries. The fluidisation gas splits the solid particles (both oxygen carriers and coke deposited catalysts from the centre to the walls (Figure 6a-c). The distribution of the fluidisation gas (CO_2) mixes the oxygen carriers and coke deposited catalysts through the regenerator (Figure 6b). A better mixing would be possible with a higher distribution of fluidisation gas (Figure 6c).

The velocity profiles of the particles and directions are presented in Figure 7, 8a and 8b for the G1, G2 and G3, respectively. Additionally, the regenerator was divided into four zones; Zone-I represents the velocity profiles from 0 to 200 mm of height in the regenerator where the effects of gas inlet would be observed. Zone-II provides the velocity profiles from 200 to 600 mm of height in the regenerator where particle hydrodynamics in the bottom section can be observed. Zone-III is the velocity profiles from 600 to 1000 mm of height in regenerator where the particles' hydrodynamics from bottom to middle stages can be observed. The final zone is Zone-IV, which provides the velocity profiles from 1000 to 1400 mm of height in regenerator where the particles' hydrodynamics from middle to top stages can be observed. Regardless of the fluidisation gas inlet geometries, CO_2 tends to rise through the centre of the regenerator where the velocities of the solid particles (oxygen carriers modified catalysts and coke deposited catalysts) are relatively high (as seen in Figures 7 and 8). The fluidisation gas splits the solid particles from the centre to the walls (as previously demonstrated in Figure 5), which create a dilute solid phase in the centre (where the velocity of the particles is quite high) and a dense gas phase near the wall (where the velocity of the particles is quite low), which is one of the characteristic flow regimes in the circulating fluidised bed reactors [55]. These flow patterns are associated with the movement, formation and splitting of bubbles [54]. Furthermore, the solid particles near the wall tend to go down (Figures 7 and 8). As in the literature, it was also demonstrated that particles accelerate the centre of the regenerator and fall close to the wall, drawing a core-annulus flow [26]. In the conventional FCC regenerator, the distribution of airflow through the regenerator is important to make a better interaction between coke and oxygen in the conventional FCC regenerator [28]. However, in this study, this affect is not as important as in the conventional unit, since the oxygen would be released through the oxygen carriers which are well mixed with the coke deposited FCC catalyst particles in the CLC-FCC concept.

Figure 7 shows the particle velocity profiles in Geometry-1 under unsteady state (Figure 7a at 2s) and steady-state (Figure 7b at 10s) conditions. In Zone-I, the particles have a low velocity at the bottom of the regenerator and create small vortexes after the fluidisation gas enters the regenerator (Figure 7a-I) at unsteady state conditions. However, the small vortexes were gradually generating a single large vortex to create a steady flow regime by 10s (Figure 7b-I). In Zone-II, the particles in the centre rise with a high velocity while the particles near the wall go down with a low velocity, as mentioned previously (Figure 7a-II and 7b-II). Due to the counter flow of particles (rising fast in the centre and

dropping slowly near the wall), the particles create vortexes as a result of the change in particles direction (generally from dilute solid phase (up-flow) to dense solid phase (down-flow)).

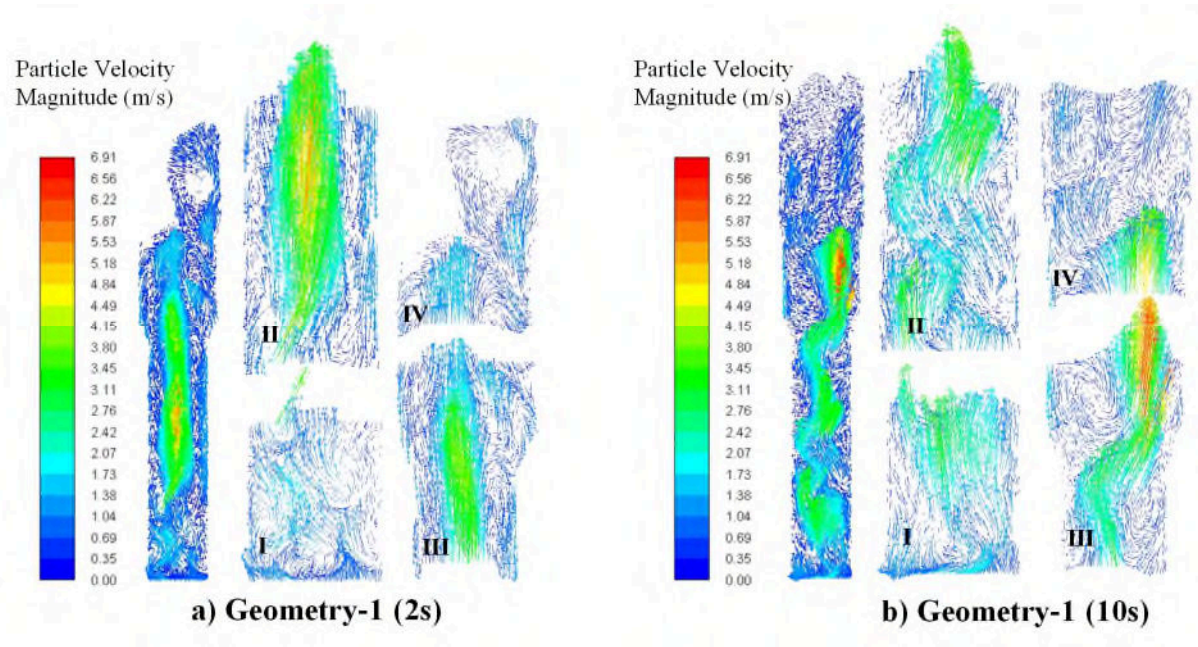

Figure 7. Velocity profiles of particles through the regenerator (Geometry-1 inlet) at a) 2s and b) 10s of simulation. The number represents Zone-I (0-200 mm of height), Zone-II (200-600 mm of height), Zone-III (600-1000 mm of height) and Zone-IV (1000-1400 mm of height).

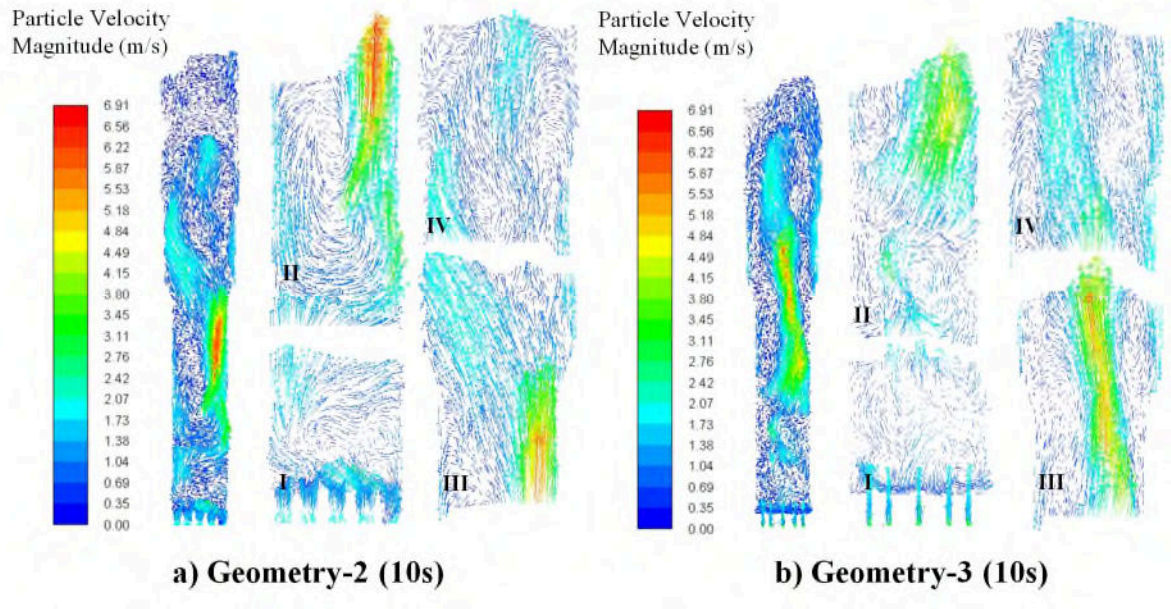

Figure 8. Velocity profiles of the particles through the regenerator in a) Geometry-2 and b) Geometry-3 at 10s of simulation. The number represents Zone-I (0-200 mm of height), Zone-II (200-600 mm of height), Zone-III (600-1000 mm of height) and Zone-IV (1000-1400 mm of height).

Furthermore, the flow regime in the centre shows a distributed shape at the steady-state condition (Figure 7b), which increases the advanced vortexes in the regenerator. In Zone-III, two fully developed vortexes were created before and after the expansion in the regenerator (Figure 7b-III) at a steady-state flow regime. These two fully developed vortexes control the flow regime passing through from the bottom to the middle section of the regenerator. The direction of the particles in this zone are also similar to Zone-II. In Zone-IV, the particles could not reach the top section of the regenerator and tend to create low-velocity vortexes due to the gravitational force on the particles (Figures 7a-IV and 7b-IV).

The distribution of the fluidisation gas (CO_2) provides a better mixing in the entrance and provides a distributed flow regime through regenerator (Figures 8a-I and 8b-I), which could contribute to the mixing of the oxygen carriers and coke deposited catalysts through the regenerator. The formation of more advanced vortexes was dependant on distributing the fluidisation gas in the inlet (Figure 8a and 8b). Additionally, the velocities of the particles also distributed evenly throughout the regenerator. The counter flow of the particles and the vortexes provide better fluidisation in the regenerator.

3.4. Superficial gas velocity

Figure 9 demonstrates the time-averaged particle volume fraction through radial distribution at the height of 250, 500, and 750 mm for the different superficial gas velocities of 0.6, 0.7, 0.8, 0.9 and 1.0 m/s. The bottom dense phases (Figure 9a) demonstrates similar trends with the different superficial gas velocities. Figure 9a shows there are insignificant effects of the superficial gas velocities on the particle volume fraction at the earlier stage of the dense phase (regenerator height of 250 mm). However, the lower superficial gas velocities (0.6-0.8 m/s) provide a much lower particle volume fraction than the higher superficial gas velocities (0.9-1.0 m/s) through the regenerator as seen in Figure 9b and 9c.

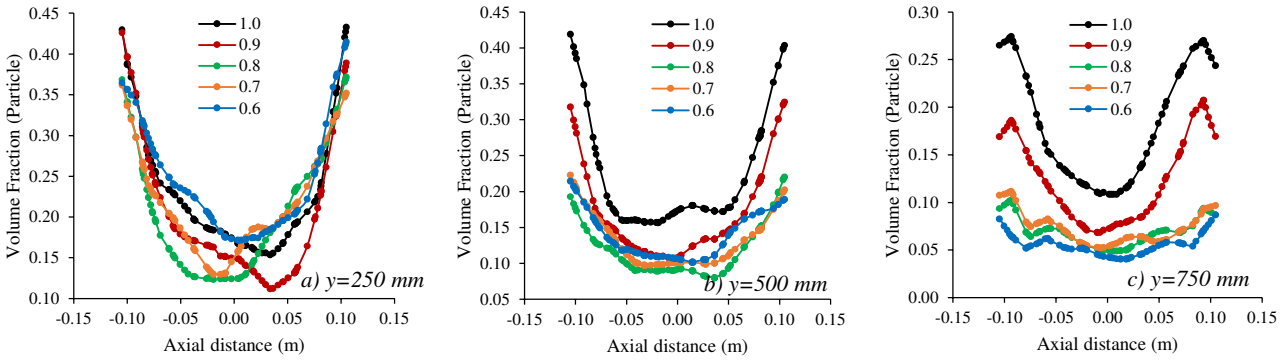

Figure 9. Time-averaged particle volume fraction through radial distribution for the superficial velocities at the regenerator height of b) 250 mm, c) 500 mm, and d) 750 mm.

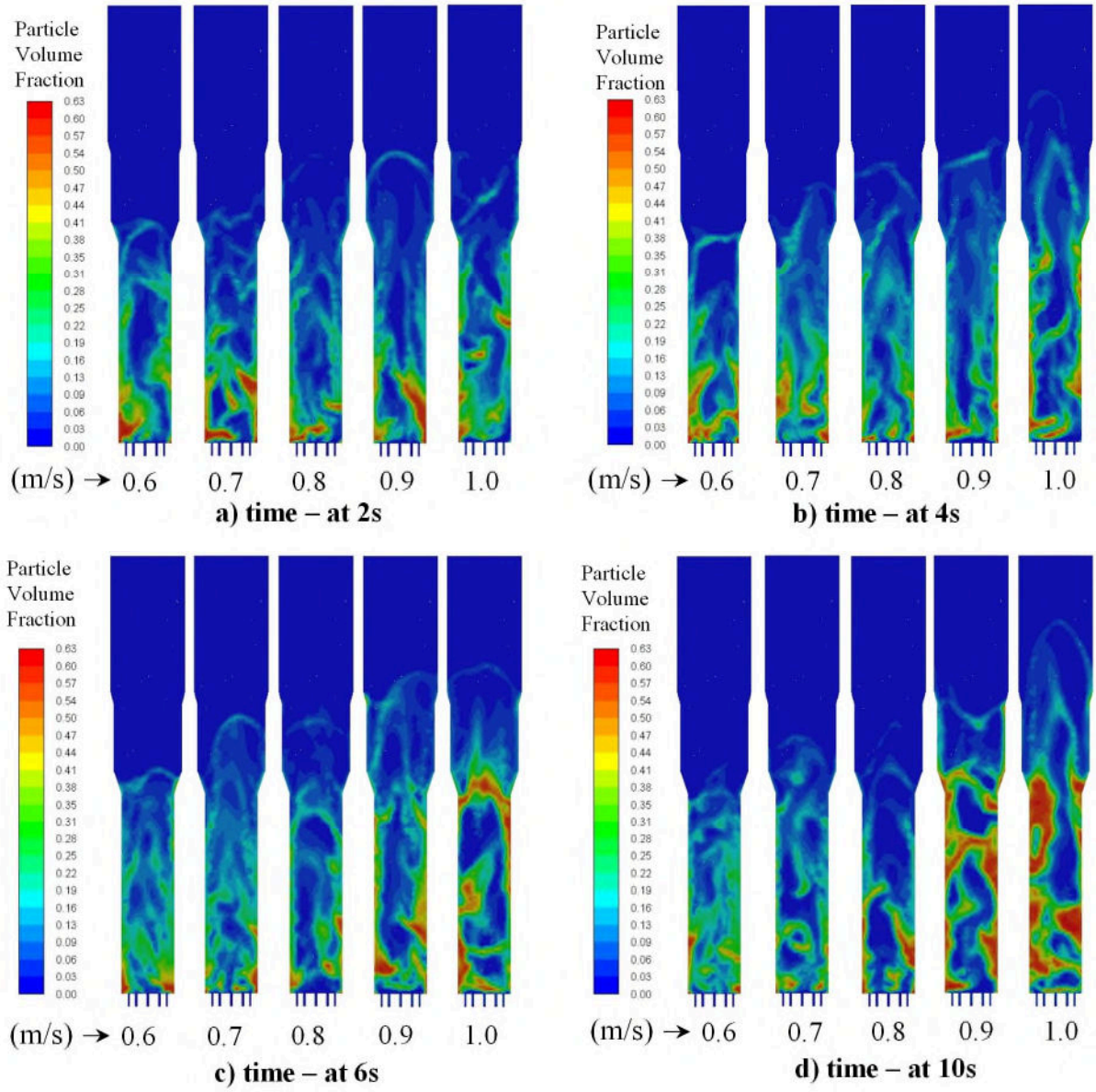

Figure 10. Instantaneous particle volume fraction profiles in the regenerator for different superficial velocities (0.6, 0.7, 0.8, 0.9, 1.0 m/s) at a) 2s, b) 4s, c) 6s, and d) 10 s of simulation.

Particle volume fraction profiles (in Figure 10) also verify the differences between low (0.6-0.8 m/s) and high (0.9-1.0 m/s) superficial gas velocities. Although the effects of superficial gas velocities on the particle volume fraction patterns have not been observed under unsteady state conditions (Figure 10a and 10b), the differences of low (0.6-0.8 m/s) and high (0.9-1.0 m/s) superficial gas velocities could be observed under the steady-state flow conditions (Figure 10c-d). Regardless of the superficial gas velocity differences, the fluidisation gas splits the oxygen carrier modified catalysts and coke deposited catalysts from the centre to the walls (as previously demonstrated in Section 3.2 and 3.3), which is the characteristic flow regime in the circulating fluidised bed reactors (a dilute solid phase in the centre, a dense gas phase near the wall). This flow regime, improves the oxygen carrier to coke contact rate.

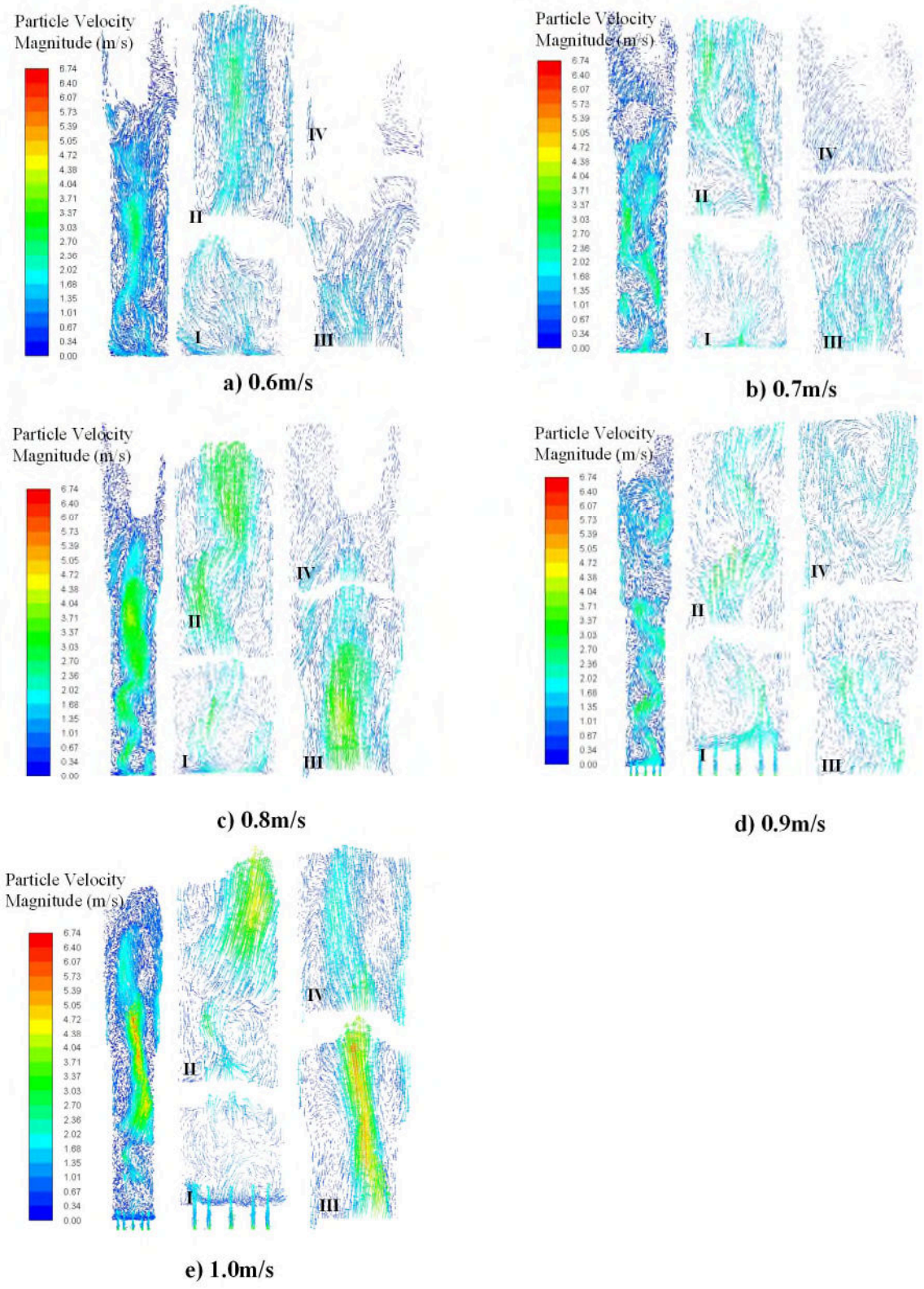

Figure 11. Velocity vector profiles of particle phase in the regenerator for the superficial velocity of a) 0.6 m/s, b) 0.7 m/s, c) 0.8 m/s, d) 0.9 m/s and e) 1.0 m/s at 10 s as steady state condition. Zone-I (-100-200 mm of height), Zone-II (200-600 mm of height), Zone-III (600-1000 mm of height) and Zone-IV (1000-1400 mm of height).

Figure 11 demonstrates the velocity vector profiles of particle phase in the regenerator for the superficial velocities of 0.6-1.0 m/s at steady-state conditions. The increase in the superficial gas velocity increase turbulence and enhances the entrainment capacity of the gas phase (Figure 11 and Figure 10), as with the conventional FCC regenerator [4, 27]. The higher superficial gas velocities (0.9-1.0 m/s, Figure 11d-e) entrained all the particles to the top of the regenerator with developed vortexes while the lower superficial gas velocities (0.63-0.8 m/s, Figure 11a-c) do not have the ability to entrain the catalyst particles. The residence time of the particles depends on the superficial gas velocity of the air in the conventional FCC regenerator since the combustion of coke (regeneration of coke deposited catalysts) depends on the oxygen in the airflow [4]. However, in the proposed CLC-FCC concept, the residence time depends on how well the coke and oxygen carriers are mixed in the regenerator, in addition to the residence time. The coke deposited on the catalysts could be expected to combust with oxygen supplied by oxygen carriers [20, 21, 43].

3.5. Flow models (Laminar and Turbulent)

Figure 12 shows the axial bed density profiles predicted by the simulation with laminar and turbulent flow models with Geometry-3 at a superficial gas velocity of 1.0 m/s. The axial bed density profiles for these two flow models demonstrate no significant differences. Both flow models (turbulent and laminar) are therefore applicable for the prediction of hydrodynamics in the dense phase of the regenerator.

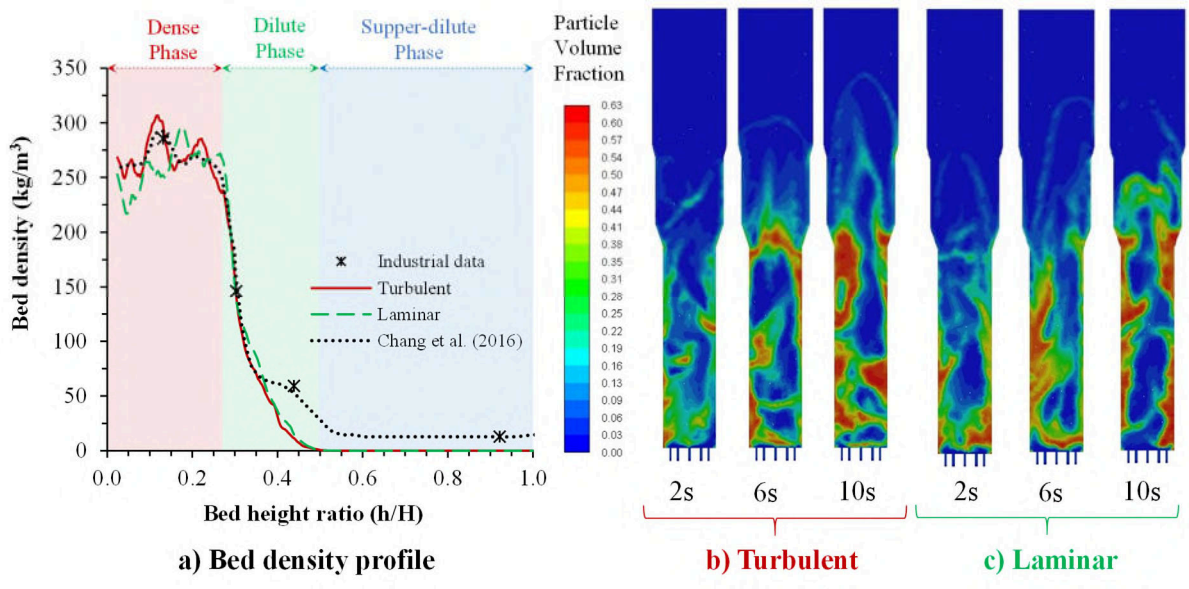

Figure 12. a) The axial bed density profiles predicted by laminar and turbulent flow regimes under the following simulation conditions (Geometry-3, superficial gas velocity of 1.0 m/s, 6-10 s of steady-state time). Particle volume fraction profiles simulated by b) Turbulent and c) Laminar flow regimes.

Gao et al.[41] and Chang et al. [26] also presented similar results, where the dense phase at the bottom of the regenerator (the bubbling/turbulent fluidised beds) exhibited low Reynolds numbers, resulting in

a low turbulent interaction in the flow regimes. Although both flow models predicted similar axial solid velocities, the laminar flow model predicted a better match with the experimental data in the high-density circulating-fluidised bed riser [55]. The turbulent flow model predicted a higher solid volume fraction at the centre in the fluidised bed riser [55]. There was no significant difference observed in the particle volume fraction profiles in the regenerator of CLC-FCC (Figure 12b and 12c), which could be attributed to the different hydrodynamics in fluidised bed riser reactor and bubbling/turbulent fluidised bed reactor. As the hydrodynamics are more sensitive to the restitution coefficient than flow models and kinetic theories [41].

In summary, the optimisation of inlet geometry (to achieve a better fluidisation gas distribution at the entrance) is crucially important for better mixing of oxygen carriers and coke deposited catalysts in the regenerator. Additionally, the mixing of oxygen carriers and coke deposited catalysts would be enhanced by the optimisation of the superficial gas velocity. Coke combustion would be enhanced improving the inlet configurations, gas-solid interaction and prolonged reaction time [26, 27]. Whilst there is no analysis of reaction mechanisms in this study, these vortexes and well-mixed fluidisation of solid particles could contribute to the regeneration of coke with oxygen carriers. The flow models (turbulent and laminar) predict similar axial bed density profiles which are also in line with the industrial data of a conventional FCC regenerator. The findings of this study suggest that CFD can potentially be used for further investigation to predict the applicability of CLC in FCC units and could provide detailed information for any modifications that would be necessary to optimise the regenerator in a CLC-FCC concept.

4. Conclusions

In this study, the potential impact of the CLC modification on the hydrodynamics of the FCC regenerator was investigated and the results comparatively discussed with the conventional FCC regenerator using the CFD analysis based on Eulerian model with the kinetic theory of granular flow.

- Conventional drag models (Syamlal-O'Brien and Gidaspow) can provide the same axial bed density profiles for CLC-FCC regenerator with the industrial data of conventional FCC regenerator: a dense phase (250-300 kg/m^3) at the bottom of the regenerator, a dilute phase in the middle of the regenerator. However, the dilute phase of the conventional FCC regenerator was disappeared in the CLC-FCC regenerator, which was attributed to the changes in the physicochemical properties of the novel FCC catalyst modified by oxygen cariers.
- The distribution geometries demonstrate a near axisymmetric radial distribution based on the time-averaged volume fraction. Regardless of the fluidisation inlet geometries, the fluidisation gas (CO_2) tends to increase through the centre of the regenerator where the mass flux of the solid particles (oxygen carriers modified catalysts and coke deposited catalysts) is relatively high. Creating a higher

gas distribution through the inlet of the regenerator (Geometry-3) provides better mixing of solid particles in the entrance and creates a distributed flow regime through the dense and dilute phases.

- The increase in the superficial gas velocity impact on the degree of turbulence to enhance entrainment in the gas phase. Increasing superficial gas velocity and pressure will increase coke combustion efficiency. Higher superficial gas velocities (0.9 m/s and 1.0 m/s) therefore provide a better mixture creating vortexes that allow well-mixed phases of oxygen carriers modified catalysts and coke deposited catalyst thoughout the regenerator.

As future work, detailed chemical and thermal CFD analyses could be investigated to optimise the residence time of the solid particles (both cokes deposited catalysts and oxygen carriers modified catalysts) in the regenerator of CLC-FCC concept by applying burnout kinetic models. Furthermore, the impact of carrier gas (CO_2) and flue gas concentration (mainly CO_2 and H_2O, potentially O_2 and CO) could be predicted from the combustion of coke with oxygen carriers (CuO) at various conditions. The regenerator inventory and catalyst circulation flowrates still require optimisation as the CLC-FCC concept requires additional oxygen carrier modified catalyst particles in the regenerator as an oxygen supply.

CRediT authorship contribution statement

F. Güleç: Conceptualisation, Investigation, Formal analysis, Visualisation, Validation, Writing - original draft, Writing - review & editing. **A. Erdoğan:** Conceptualisation, Investigation, CFD simulation, Formal analysis, Visualisation, Validation, Writing - original draft, Writing - review & editing. **P. T. Clough:** Conceptualisation, Methodology, Formal analysis, Visualisation, Reviewing and Editing. **E. Lester:** Conceptualisation, Methodology, Formal analysis, Visualisation, Reviewing and Editing.

Abbreviations

CLC : Chemical Looping Combustion

CLOU : CLC with oxygen uncoupling

CO_2 : Carbon dioxide

Co_3O_4 : Cobalt (II, III) oxide

CoO : Cobalt (II) oxide

Co : Cobalt

CuO : Copper (II) oxide

Cu_2O : Copper (I) oxide

Cu : Copper

CH_4 : Methane

C_{1-2} : Dry Gas

C_{3-4} : Liquefied petroleum gas – LPG

C_{5-13} : Gasoline

ECat : Equilibrium catalyst

FCC : Fluid Catalytic Cracking

HC : Hard coke

Mn_2O_3 : Manganese (III) oxide

Mn_3O_4 : Manganese (II,III) oxide

MnO : Manganese (II) oxide

Me_nO_m : Oxidised metal oxide

Me_nO_{m-1}: Reduced metal oxide

N_2 : Nitrogen

O_2 : Oxygen

SC : Soft coke

VGO : Vacuum gas oil

WHSG : Waste heat steam generator

Greek letters

α : Volume fraction

ε : Dissipation rate of turbulent kinetic energy

k : Turbulent kinetic energy

μ : Dynamic viscosity

$\mu_{t,g}$: Gas-phase turbulent viscosity

$\mu_{eff,g}$: Effective viscosity of gas phase

μ_s : Shear viscosity for solid particles

ρ : Density

σ_k, σ_ε : Turbulent Prandtl numbers

γ_s : Collisional dissipation of energy

λ_s : Solid-phase bulk viscosity

λ_g : Bulk viscosity of gas phase

ϕ_{gs} : Transfer of fluctuating kinetic energy

v' : Fluctuating velocity of the solid-phase particles

Θ : Granular temperature

Π_k, Π_ε : Turbulent exchange terms describing the influence of the solid phase on the gas phase

Γ_Θ : Coefficient of granular diffusion

Notations

C_D : Drag coefficient

d_s : Particle diameter, μm

d_p^* : Effective mean particle diameter, μm

e : Coefficient of elastic restitution

g_i : Acceleration due to gravity, m/s_2

g_0 : Radial distribution function

h : Bed height, m

P : Pressure, Pa

r : Radial direction

R : Diameter of bed, mm

C_μ : Turbulence model constant,

C_2 : Empirical model constants

$C_{1\varepsilon}$: Empirical model constants

$C_{3\varepsilon}$: Turbulence model constant

G_k : Turbulent kinetic energy produced

$\bar{I}$: Unit tensor

Re : Reynolds number

U : Phase-weighted velocity

References

[1] G. Tang, A. Silaen, B. Wu, D. Fu, D. Agnello-Dean, J. Wilson, Q. Meng, S. Khanna, C.Q. Zhou, Numerical study of a fluid catalytic cracking regenerator hydrodynamics, Powder Technology, 305 (2017) 662-672.

[2] G. Tang, A.K. Silaen, B. Wu, D. Fu, D. Agnello-Dean, J. Wilson, Q. Meng, S. Khanna, C.Q. Zhou, Numerical simulation and optimization of an industrial fluid catalytic cracking regenerator, Applied Thermal Engineering, 112 (2017) 750-760.

[3] D.J. Rawlence, K. Gosling, FCC catalyst performance evaluation, Applied Catalysis, 43 (1988) 213-237.

[4] A. Azarnivand, Y. Behjat, A.A. Safekordi, CFD simulation of gas–solid flow patterns in a downscaled combustor-style FCC regenerator, Particuology, 39 (2018) 96-108.

[5] R. Sadeghbeigi, Fluid Catalytic Cracking Handbook, in, Gulf Publishing Company, Houston, 2000.

[6] D.S. Jones, P.P. Pujadó, Handbook of petroleum processing, Springer Science & Business Media, 2006.

[7] W.-C. Cheng, G. Kim, A. Peters, X. Zhao, K. Rajagopalan, M. Ziebarth, C. Pereira, Environmental fluid catalytic cracking technology, Catalysis Reviews, 40 (1998) 39-79.

[8] EPA, Available and emerging technologies for reducing GHG emissions from petroleum refining, in, U.S. Environmental Protection Agency, 2010.

[9] J. van Straelen, F. Geuzebroek, N. Goodchild, G. Protopapas, L. Mahony, CO2 capture for refineries, a practical approach, International Journal of Greenhouse Gas Control, 4 (2010) 316-320.

[10] T. Kuramochi, A. Ramírez, W. Turkenburg, A. Faaij, Comparative assessment of CO2 capture technologies for carbon-intensive industrial processes, Progress in energy and combustion science, 38 (2012) 87-112.

[11] IEA, Clean Energy Progress, Industry-CCS annex, in, IEA Statistic, 2013.

[12] J. van Straelen, F. Geuzebroek, N. Goodchild, G. Protopapas, L. Mahony, CO2 capture for refineries, a practical approach, Energy Procedia, 1 (2009) 179-185.

[13] P. Peng, Y. Zhuang, The evaluation and comparison of carbon dioxide capture technologies applied to FCC flue gas, in: Advanced Materials Research, Trans Tech Publ, 2012, pp. 1479-1482.

[14] R. Digne, F. Feugnet, A. Gomez, A Technical and Economical Evaluation of CO2 Capture from Fluidized Catalytic Cracking (FCC) Flue Gas, Oil & Gas Science and Technology–Revue d'IFP Energies nouvelles, 69 (2014) 1081-1089.

[15] T. Melien, S.B. Roijen, Economics, Carbon Dioxide Capture for Storage in Deep Geologic Formations, 3 (2009) 237-264.

[16] L.F. de Mello, R.D. Pimenta, G.T. Moure, O.R. Pravia, L. Gearhart, P.B. Milios, T. Melien, A technical and economical evaluation of CO2 capture from FCC units, Energy Procedia, 1 (2009) 117-124.

[17] F. Sher, M.A. Pans, C. Sun, C. Snape, H. Liu, Oxy-fuel combustion study of biomass fuels in a 20 kWth fluidized bed combustor, Fuel, 215 (2018) 778-786.

[18] F. Güleç, W. Meredith, C.-G. Sun, C.E. Snape, Selective low temperature chemical looping combustion of higher alkanes with Cu-and Mn-oxides, Energy, 173 (2019) 658-666.

[19] F. Güleç, W. Meredith, C.-G. Sun, C.E. Snape, A novel approach to CO2 capture in Fluid Catalytic Cracking—Chemical Looping Combustion, Fuel, 244 (2019) 140-150.

[20] F. Güleç, W. Meredith, C.E. Snape, Progress in the CO2 Capture Technologies for Fluid Catalytic Cracking (FCC) Units—A Review, Frontiers in Energy Research, 8 (2020).

[21] F. Güleç, W. Meredith, C.-G. Sun, C.E. Snape, Demonstrating the applicability of chemical looping combustion for the regeneration of fluid catalytic cracking catalysts, Chemical Engineering Journal, 389 (2020) 124492.

[22] Y. Yan, K. Wang, P.T. Clough, E.J. Anthony, Developments in calcium/chemical looping and metal oxide redox cycles for high-temperature thermochemical energy storage: A review, Fuel Processing Technology, 199 (2020) 106280.

[23] J.C. Hicks, J.H. Drese, D.J. Fauth, M.L. Gray, G. Qi, C.W. Jones, Designing adsorbents for CO2 capture from flue gas-hyperbranched aminosilicas capable of capturing CO2 reversibly, Journal of the American Chemical Society, 130 (2008) 2902-2903.

[24] P. Wang, N. Means, D. Shekhawat, D. Berry, M. Massoudi, Chemical-looping combustion and gasification of coals and oxygen carrier development: a brief review, Energies, 8 (2015) 10605-10635.

[25] Y. Cao, B. Casenas, W.-P. Pan, Investigation of chemical looping combustion by solid fuels. 2. Redox reaction kinetics and product characterization with coal, biomass, and solid waste as solid fuels and CuO as an oxygen carrier, Energy & Fuels, 20 (2006) 1845-1854.

[26] J. Chang, J. Zhao, K. Zhang, J. Gao, Hydrodynamic modeling of an industrial turbulent fluidized bed reactor with FCC particles, Powder Technology, 304 (2016) 134-142.

[27] J. Chang, G. Wang, X. Lan, J. Gao, K. Zhang, Computational investigation of a turbulent fluidized-bed FCC regenerator, Industrial & Engineering Chemistry Research, 52 (2013) 4000-4010.

[28] B. Amblard, R. Singh, E. Gbordzoe, L. Raynal, CFD modeling of the coke combustion in an industrial FCC regenerator, Chemical Engineering Science, 170 (2017) 731-742.

[29] R. Singh, E. Gbordzoe, Modeling FCC spent catalyst regeneration with computational fluid dynamics, Powder Technology, 316 (2017) 560-568.

[30] A. Fluent, Ansys fluent theory guide, ANSYS Inc., USA, 15317 (2011) 724-746.

[31] D. Gidaspow, Multiphase flow and fluidization: continuum and kinetic theory descriptions, Academic press, 1994.

[32] J. Sinclair, R. Jackson, Gas-particle flow in a vertical pipe with particle-particle interactions, AIChE journal, 35 (1989) 1473-1486.

[33] J. Ding, D. Gidaspow, A bubbling fluidization model using kinetic theory of granular flow, AIChE journal, 36 (1990) 523-538.

[34] J.M. DallaValle, Micromeritics: the technology of fine particles, Pitman Publishing Limited, 55 (1948) 151.

[35] J. Garside, M.R. Al-Dibouni, Velocity-voidage relationships for fluidization and sedimentation in solid-liquid systems, Industrial & engineering chemistry process design and development, 16 (1977) 206-214.

[36] J.T. Richardson, Sedimentation and fluidisation: Part I, Transactions of the Institution of Chemical Engineers, 32 (1954) 35-53.

[37] M. Syamlal, T.J. O'Brien, Computer simulation of bubbles in a fluidized bed, in: AIChE Symp. Ser, Publ by AIChE, 1989, pp. 22-31.

[38] C. Lun, S.B. Savage, D. Jeffrey, N. Chepurniy, Kinetic theories for granular flow: inelastic particles in Couette flow and slightly inelastic particles in a general flowfield, Journal of fluid mechanics, 140 (1984) 223-256.

[39] D. Gidaspow, R. Bezburuah, J. Ding, Hydrodynamics of circulating fluidized beds: kinetic theory approach, in, Illinois Inst. of Tech., Chicago, IL (United States). Dept. of Chemical …, 1991.

[40] O. Simonin, P. Viollet, Modelling of turbulent two-phase jets loaded with discrete particles, Phenomena in multiphase flows, 1990 (1990) 259-269.

[41] J. Gao, X. Lan, Y. Fan, J. Chang, G. Wang, C. Lu, C. Xu, CFD modeling and validation of the turbulent fluidized bed of FCC particles, AIChE journal, 55 (2009) 1680-1694.

[42] R. Sadeghbeigi, Fluid catalytic cracking handbook: An expert guide to the practical operation, design, and optimization of FCC units, Butterworth-Heinemann, 2020.

[43] F. Güleç, Demonstrating the applicability of chemical looping combustion for fluid catalytic cracking unit as a novel CO2 capture technology, in: Chemical Engineering, University of Nottingham, 2020.

[44] T. Mattisson, A. Järdnäs, A. Lyngfelt, Reactivity of some metal oxides supported on alumina with alternating methane and oxygen application for chemical-looping combustion, Energy & Fuels, 17 (2003) 643-651.

[45] J.D. Alzate Hernández, CFD simulation of an industrial FCC regenerator, in, Universidad Nacional DE Colombia-Sede Medellin, 2016.

[46] X. Wang, B. Jin, Y. Zhang, W. Zhong, S. Yin, Multiphase computational fluid dynamics (CFD) modeling of chemical looping combustion using a CuO/Al2O3 oxygen carrier: effect of operating conditions on coal gas combustion, Energy & Fuels, 25 (2011) 3815-3824.

[47] N.A. Schiller L, A drag coefficient correlation, Zeit. Ver. Deutsch. Ing., 77 (1933) 318-320.

[48] Y.P. Tsuo, D. Gidaspow, Computation of flow patterns in circulating fluidized beds, AIChE Journal, 36 (1990) 885-896.

[49] J. Adánez, P. Gayán, J. Celaya, L.F. de Diego, F. García-Labiano, A. Abad, Chemical looping combustion in a 10 kWth prototype using a CuO/Al2O3 oxygen carrier: Effect of operating conditions on methane combustion, Industrial & engineering chemistry research, 45 (2006) 6075-6080.

[50] L.F. De Diego, P. Gayán, F. García-Labiano, J. Celaya, A. Abad, J. Adánez, Impregnated CuO/Al2O3 oxygen carriers for chemical-looping combustion: avoiding fluidized bed agglomeration, Energy & Fuels, 19 (2005) 1850-1856.

[51] R. Siriwardane, H. Tian, G. Richards, T. Simonyi, J. Poston, Chemical-looping combustion of coal with metal oxide oxygen carriers, Energy & Fuels, 23 (2009) 3885-3892.

[52] S. Chuang, J. Dennis, A. Hayhurst, S. Scott, Development and performance of Cu-based oxygen carriers for chemical-looping combustion, Combustion and Flame, 154 (2008) 109-121.

[53] P. Li, X. Lan, C. Xu, G. Wang, C. Lu, J. Gao, Drag models for simulating gas–solid flow in the turbulent fluidization of FCC particles, Particuology, 7 (2009) 269-277.

[54] J. Gao, X. Lan, Y. Fan, J. Chang, G. Wang, C. Lu, C. Xu, Hydrodynamics of gas–solid fluidized bed of disparately sized binary particles, Chemical Engineering Science, 64 (2009) 4302-4316.

[55] A. Almuttahar, F. Taghipour, Computational fluid dynamics of high density circulating fluidized bed riser: study of modeling parameters, Powder Technology, 185 (2008) 11-23.

[56] S. Zimmermann, F. Taghipour, CFD modeling of the hydrodynamics and reaction kinetics of FCC fluidized-bed reactors, Industrial & engineering chemistry research, 44 (2005) 9818-9827.

Investigation of the hydrodynamics in the regenerator of fluid catalytic cracking unit integrated by chemical looping combustion

Fatih Güleç[1,2]*, Ahmet Erdogan[3], Peter T. Clough[2], Edward Lester[1]

[1]*Advanced Materials Research Group, Faculty of Engineering, University of Nottingham, Nottingham, NG7 2RD, UK.*
[2]*Energy and Power Theme, School of Water, Energy and Environment, Cranfield University, Cranfield, MK43 0AL, UK*
[3]*Mechanical Engineering, Faculty of Engineering, Inonu University, 44280 Malatya, Turkey*
**Corresponding Author: Fatih.Gulec1@nottingham.ac.uk, Gulec.Fatih@outlook.com*

Appendix A

In order to determine the material balance for the proposed CLC-FCC unit, a case study is conducted with a medium size of FCC unit having a feed rate of 50,000 barrels per day (bpd). In this case study, the cracking reaction of vacuum gas oil (VGO) was assumed to investigated over the ~12 wt.% Cu_2O modified ECat and the product distributions found in the case study held by Sadeghbeigi [1] in which the conversion of VGO is 72 wt.% [1]. The conversion of VGO were updated regarding to the experimental results presented in our previous studies [2, 3], as presented in Table A1.

Table A1. Product distribution from the case study and updated values for the proposed CLC-FCC unit.

Feed and Product distribution	Case study*		CLC-FCC unit**		Distribution Differences
	Flowrate (ton/h)	Distribution (wt. %)	Flowrate (ton/h)	Distribution (wt. %)	
Fresh Feed (50000 bpd)	~418.69	-	~418.69	-	-
Conversion	72	-	70	-	2.0
Cracking Products					
Light gases	13.35	3.19	13.35	3.2	0.01
LPG	63.30	15.12	56.94	13.6	-1.52
Gasoline	208.07	49.70	197.62	47.2	-2.50
LCO	86.97	20.77	86.97	20.8	0.03
HCO + Slurry oil	29.64	7.08	40.19	9.6	2.52
Coke	17.34	4.14	23.44	5.6	1.46
Total Hydrocarbon	418.69	100	418.53	100	-

* The values collected from the case study [1].
** Updated values using the experimental results presented in our previous works [3-5].

Appendix B

The minimum fluidising velocity (u_{mf}) was determined using the same procedure presented by Kunii and Levenspiel [6] and Yang [7]. If the particle Reynolds number at minimum fluidising conditions lower than 20, the minimum fluidising velocity can be determined using Eq 1.

$$u_{mf} = \frac{d_p^2(\rho_s - \rho_g)g}{150\mu} * \frac{\varepsilon_{mf}^3 \phi_s^2}{1-\varepsilon_{mf}} \qquad Re_{p,mf} < 20 \qquad (1)$$

$$Re_{p,mf} = \frac{d_p u_{mf} \rho_g}{\mu} \qquad (2)$$

$$Re_{p,sf} = \frac{d_p u_{sf} \rho_g}{\mu_g} \qquad (3)$$

u_{mf}: Minimum fluidisation velocity (cm/s)
d_p: Particle diameter (cm)
ρ_s: Density of solids (g/cm^3)
ρ_g: Gas density (g/cm^3)
g: Acceleration of gravity (980 cm/s^2)
μ: Viscosity of gas (g/m.s)
ε_{mf}: Void fraction in a bed at minimum fluidising conditions
$\emptyset_s$: Sphericity of a particle (dimensionless)
$Re_{p,mf}$: Particle Reynolds number at minimum fluidising conditions (dimensionless)
$Re_{p,sf}$: Particle Reynolds number at superficial fluidising velocities (dimensionless)

The particle diameter of the ECat catalysts (d_p) was measured about 65 microns (0.0065 cm) by sieving method. Further, it was assumed that the particle diameter was not dramatically changed after the impregnation of oxygen carriers neither coke deposition. The density of solid (ρ_s) for Cu-based experiments was assumed an average density of I-CuO/ECat (2.84 g/cm^3) and I-Cu/ECat (2.77 g/cm^3), which is 2.80 g/cm^3. The gas density (ρ_g) and viscosity (μ) for carrier CO_2 were found as 0.001118 g/cm^3 and 0.00023 g/cm s, respectively. The catalyst pellets are spherical, thus, the sphericity of particle ($\emptyset_s$) must be 1.0 (the fragmentation of the catalyst particle after oxygen carrier impregnation was neglected). The void fraction in the bed can be read as 0.459 from the chart, "ε_{mf} as a function of d_p for fine particles" presented by Xu and Zhu [8].

From Eq 1, the minimum fluidisation velocity can be determined as; u_{mf} =0.60 cm/s for the regenerator of a mixture of Coke/I-Cu/ECat with I-CuO/ECat. From Eq 2, the particle Reynolds numbers can be found as; $Re_{p,mf}$ = 0.0189 for the minimum fluidising velocity of 0.60 cm/s. Thus, the Reynolds number is lower than 20, which means Eq 1 is suitable for the calculation of minimum fluidising velocity.

Specific Reynold numbers for each superficial fluidisation velocity were determined using Eq 3 and the Specific Reynold numbers were determined as 1.89, 2.21, 2.52, 2.84, 3.15 for the superficial fluidisation velocities of 0.6, 0.7, 0.8, 0.9 and 1.0 m/s, respectively.

References

[1] R. Sadeghbeigi, Fluid Catalytic Cracking Handbook, in, Gulf Publishing Company, Houston, 2000.
[2] F. Güleç, W. Meredith, C.E. Snape, Progress in the CO2 Capture Technologies for Fluid Catalytic Cracking (FCC) Units—A Review, Frontiers in Energy Research, 8 (2020).
[3] F. Güleç, W. Meredith, C.-G. Sun, C.E. Snape, Demonstrating the applicability of chemical looping combustion for the regeneration of fluid catalytic cracking catalysts, Chemical Engineering Journal, 389 (2020) 124492.
[4] F. Güleç, W. Meredith, C.-G. Sun, C.E. Snape, A novel approach to CO2 capture in Fluid Catalytic Cracking—Chemical Looping Combustion, Fuel, 244 (2019) 140-150.
[5] F. Güleç, Demonstrating the applicability of chemical looping combustion for fluid catalytic cracking unit as a novel CO2 capture technology, in: Chemical Engineering, University of Nottingham, 2020.
[6] D. Kunii, O. Levenspiel, Fluidization engineering, Elsevier, 2013.
[7] W.-c. Yang, Handbook of fluidization and fluid-particle systems, CRC press, 2003.

[8] C.C. Xu, J. Zhu, Prediction of the minimum fluidization velocity for fine particles of various degrees of cohesiveness, Chemical Engineering Communications, 196 (2008) 499-517.

Investigation of the hydrodynamics in the regenerator of fluid catalytic cracking unit integrated by chemical looping combustion

Güleç, Fatih

2021-08-25

Güleç F, Erdogan A, Clough PT, Lester E. (2021) Investigation of the hydrodynamics in the regenerator of fluid catalytic cracking unit integrated by chemical looping combustion. Fuel Processing Technology, Volume 223, December 2021, Article number 106998
https://doi.org/10.1016/j.fuproc.2021.106998